Pressure-induced lattice instability and solid-state amorphization

A. G. Lyapin and V. V. Brazhkin
Institute for High Pressure Physics, Russian Academy of Sciences, Troitsk, Moscow region, 142092, Russia
(Received 26 September 1995; revised manuscript received 20 June 1996)

Using semiempirical atomic potentials, we consider the mechanical and geometrical origins of pressure-induced instability for open-packed structures (bcc, sc, and diamondlike) in the framework of a classical static ($T=0$) lattice. The destabilizing role of central repulsive forces has been shown for molecular, ionic, and covalent compounds. Two types of elastic instability connected with the symmetry of nearest atomic environment and with the internal strain in an elementary cell have been revealed. The modified valence force field model is applied for calculating the high-pressure lattice dynamics of diamond and zinc-blende semiconductors. The force field model is based on the Morse form of pair potential and distance scaling of the second-order constants. It is shown that the absolute instability of diamond structure is caused by phonon softening on the boundary of the Brillouin zone, and under compression a thermally frozen diamondlike lattice may transform to a disordered state both from crystallographic and kinetic reasons. The geometrical criterion for soft modes under hydrostatic compression (relative atomic displacements are perpendicular to the bonds) is also discussed. [S0163-1829(96)04037-4]

I. INTRODUCTION

Solid-state amorphization (SSA), which may be caused by different driving forces, such as ion implantation, high-energy particle irradiation, chemical diffusion, mechanical alloying, etc., is a very promising phenomenon for the physics of disordered condensed matter.[1] High-pressure SSA (Ref. 2) is a special case, when a homogeneous crystal spontaneously transforms to a disordered solid, and it has a great technological potential for production of bulk amorphous materials. The different pressure-induced amorphization transformations, observed under compression [H_2O, SiO_2, etc. (Refs. 3 and 4)], decompression [H_2O, Si, Ge, GaAs, etc. (Refs. 5–7)], or upon heating [GaSb, SiO_2, etc. (Refs. 2 and 8)], have two common basic features—a deep metastability of the initial crystal before the onset of disordering and a similarity between the short-range order structures (SROS) of the amorphous phase obtained and the crystalline modification, which is stable at the amorphization conditions.

A number of experimental observations—heat release during amorphization and small activation energy,[2,8] clearly distinguish the high-pressure SSA from a conventional order-disorder transition, like melting. Amorphous phases produced using the high-pressure SSA method also display anomalous anisotropy of physical properties,[9,10] which are not observable in conventional glasses prepared by ordinary methods (glass forming, quenching from the melt, evaporation, etc.). This anisotropy can be interpreted in the framework of the ''memory'' effects of the initial crystal orientation before the SSA.[10,11] The lamellar structure of the disordered SiO_2 phase in the SSA intermediate stages[12] and the recent report on antiferromagnetism in the amorphous substance produced by the SSA (Ref. 13) may well be considered as still another manifestation of anisotropy effects during the SSA.

The theoretical interpretation of the SSA proceeds from the idea of Mishima *et al.*[3] about the SSA as a cold melting process. The parallels between thermodynamic melting and heterogeneous formation of an amorphous phase and, on the other hand, between ''mechanical'' melting (instability on spinodal) and homogeneous amorphization were recognized later.[14] In recent years lattice instability as a mechanism triggering amorphization became the most popular approach. The molecular-dynamics calculations for ice, α-quartz, and berlinite[15–17] have shown the direct relation between amorphization and significant softening of elastic constants. The formulation of generalized elastic stability criteria[18,19] derived from stress-strain relations allows us to predict quantitatively the symmetry and the onset of mechanical lattice instability. The molecular-dynamics simulation has directly confirmed the validity of these criteria.[18,19] In the case of α-quartz, the *ab initio* pseudopotential calculation has given vanishing of a stiffness elastic eigenconstant in the pressure range, where the disordering collapse had been observed experimentally.[20,21] The lattice instability approach gives a qualitative understanding of anisotropy effects during the SSA assuming a direct connection between the symmetry of the soft mode and real atomic movements.

For a number of SSA techniques the 30–60 % softening of elastic constants before the onset of amorphization has been confirmed experimentally.[22] An experimental study of the crystal elastic behavior before amorphization appears to have been realized on ice,[23] where the $\sim$12% decrease of the polycrystalline shear modulus was observed. Thus, there is both experimental and theoretical evidence for a relation between the high-pressure SSA, elastic lattice softening, and instability.

There has been significant progress in the understanding of SSA driving forces, but the development of a general theory on the high-pressure SSA is far from being complete. The effect of pressure and temperature on the SSA process as well as the relation between the symmetry of an unstable mode and the type of transformation are only at the beginning of their recognition. Although the generalized stability criteria for a homogeneous lattice under compression had been formulated,[18,19] the detailed criteria taking into consid-

eration a lattice geometry and an atomic forces potential as an input, which may allow us to predict instability or amorphization, are practically absent except for the calculations for certain particular substances.

In the current paper we consider a special case of open-packed lattices under compression. We imply here that the structure is open packed, when it may be packed to a denser phase (with the same distances to nearest neighbors) under pressure. Our consideration is restricted by the condition $Z \leqslant 8$, but, in the case of metals, it is doubtful that bcc crystals ($z=8$) are open packed. In Sec. II we shall apply the generalized stability criteria to simple cubic and bcc structures. This consideration will allow us to clear up the destabilizing role of the central repulsive forces closely connected with the symmetry and geometry of the structure. The qualitative conclusions will be supported by the numerical analysis of alkali halides using empirical potentials.

In Sec. III we shall examine the elastic and vibration stability of the diamondlike structure in the case of tetrahedral semiconductors. This case is of great interest because the SSA transformation has been recently discovered in zinc blende BAs.[24] The molecular-dynamics simulation of tetrahedral covalent alloy SiC has also displayed a crystal-to-amorphous transition, caused by the elastic instability under compression.[25] We shall modify the conventional valence force field model by taking into account: (i) the anharmonic character of central overlap forces under pressure; (ii) the contribution of electronic density increase under compression into third-order force constants; and (iii) flattening of the transverse-acoustic branch at the Brillouin-zone boundary. The chosen potential will be tested by the calculation of Grüneisen constants and pressure derivatives of stiffness elastic constants. The minimum critical pressure from different stability criteria will be found corresponding to the TA(X) phonon mode for a number of tetrahedral semiconductors.

In Sec. IV we shall discuss the relations between the symmetry of instability and the solid-state transition actually observed. In the case of a diamondlike structure the suggestion about the possibility of solid-state amorphization in general case under compression will be advanced proceeding from crystallographic considerations. The analysis of geometrical relations for different soft modes will give a new insight into the nature of unstable modes in compressed open-packed lattices. Finally, we shall briefly repeat in Sec. V the basic qualitative results supported by quantitative calculations in Secs. II and III.

II. INSTABILITY OF SIMPLE CUBIC AND BCC LATTICES UNDER COMPRESSION

For given P,T conditions the equilibrium atomic configuration in a crystal, $\mathbf{X}=\mathbf{X}(P,T)$, corresponds to the minimum of Gibbs free energy $G=U-TS+PV$. For a crystal in the metastable state this minimum is evidently local. In a classical static ($T=0$) lattice the internal energy U may be considered as a potential function, $U=U(\mathbf{X})$. Introduction of a potential function for describing atomic interaction is natural, if we want to clarify the role of lattice geometry and atomic forces in lattice instability. Previously, empirical atomic potentials had been successfully applied for describing elastic and vibration properties of molecular, ionic, and covalent crystals at normal conditions, when pressure may not be taken into account. (For example, see Refs. 26 and 27.) The zero-temperature restriction in the framework of a classical lattice allows us to eliminate from consideration atomic oscillations and to use the harmonic approximation[26,28] for lattice dynamics.

The generalized elastic stability criteria for a cubic crystal under hydrostatic pressure have been proposed by Wang *et al.*[18,19] proceeding from the consideration of a stiffness coefficient tensor.[30,29] These criteria may be written in a form similar to the ordinary stability criteria of Born[26] for zero pressure:

$$c_{11}^{*}+2c_{12}^{*}>0, \quad c_{11}^{*}-c_{12}^{*}>0, \quad c_{44}^{*}>0, \tag{2.1}$$

where elastic stiffness, or stress-strain, coefficients[29] may be expressed in terms of the Gibbs free energy G and the Lagrangian strain tensor $u_{\alpha\beta}=\frac{1}{2}(\epsilon_{\alpha\beta}+\epsilon_{\beta\alpha}+\Sigma_{\gamma}\epsilon_{\gamma\alpha}\epsilon_{\gamma\beta})$, by the equation:

$$c_{\alpha\beta\gamma\lambda}^{*}=\frac{1}{V}\frac{\partial^2 G}{\partial u_{\alpha\beta}\partial u_{\gamma\lambda}}, \tag{2.2}$$

here V is the volume of crystal, indices designate x, y, or z axes, and $c_{\alpha\beta\gamma\lambda}^{*}\equiv c_{ij}^{*}$ in Voigt's notation[31] ($i,j=1,\ldots,6$). Under uniaxial tension the cubic symmetry of the stiffness coefficient tensor breaks down and the criteria (2.1) become not valid.[18]

At first, we have applied the criteria (2.1) to the simplest case of a lattice with central interatomic forces. The change of potential energy in a lattice under deformation have been calculated by Born,[26] the corresponding equation being simplified for simple cubic and bcc structures, where there is one atom per elementary cell, and the internal strain in the cell is absent. Taking into account the expressions for elastic stiffness coefficients from Refs. 18 and 19 one can obtain tetragonal and rhombohedral shear eigenconstants for a stiffness coefficient tensor:

$$\frac{1}{2}(c_{11}^{*}-c_{12}^{*})=\frac{1}{v}\sum_{i}\left[\psi''_{r^2}(r_x^4-r_x^2r_y^2)\right]_{\mathbf{r}_i}-P, \tag{2.3a}$$

$$c_{44}^{*}=\frac{2}{v}\sum_{i}\left[\psi''_{r^2}r_x^2r_y^2\right]_{\mathbf{r}_i}-P, \tag{2.3b}$$

where v is the volume of an elementary cell, $\mathbf{r}_i$ is a relative vector of the Brave lattice, and ψ''_{r^2} denotes the second derivative of pair potential as a function of r^2, $\psi''_{r^2}=\partial^2\psi(r^2)/\partial(r^2)^2$. Equations (2.3a) and (2.3b), being a particular case of the general equations,[29] may be derived from the thermodynamic Gibbs free-energy consideration.[32] The first terms in the right-hand part of Eqs. (2.3a) and (2.3b) are connected with the Born strain energy, whereas the term $-P$ appears to be due to macroscopic second-order variation of a crystal volume. The condition of crystal equilibrium $\partial G/\partial u_{\alpha\beta}=0$ gives in this case

$$P=\frac{1}{v}\sum_{i}\left[\psi'_{r^2}r_x^2\right]_{\mathbf{r}_i}. \tag{2.4}$$

Before numerical application of Eqs. (2.3) and (2.4), one should note, that sc and bcc structures with central forces are usually unstable in contrast to the close-packed fcc lattice.[26] According to Eqs. (2.1), (2.3), and (2.4), these structures remain unstable under positive pressure because there is no positive contribution from the first shell to c_{44} in the sc and to $(1/2)(c_{11}-c_{12})$ in bcc structures, whereas the first-shell contribution to the pressure is always positive. Such situation appears to be due to the multipliers $(r_x^4-r_x^2r_y^2)$ and $r_x^2r_y^2$ in the first terms of the right-hand part of Eqs. (2.3), i.e., due to the symmetry of sc and bcc lattices. The total contribution of next coordination spheres to the shear constants usually corresponds to the attraction part of interatomic potential and is negative.

To analyze the relative role of different shells we should briefly consider the elastic characteristics of virtual sc and bcc lattices with the Lennard-Jones interatomic potential $\psi(r)=4\epsilon[(\sigma/r)^{12}-(\sigma/r)^6]$ successfully describing rare-gas solids (fcc structure).[27] Calculation of the stiffness elastic constant and pressure dependence $P(d)$ becomes trivial, according to Eqs. (2.3) and (2.4), if the interaction is restricted by a sphere with radius R . The role of atoms outside of this sphere can be estimated from the approximation of continuous atomic distribution with density $n=1/v$. In this model the summing up in Eq. (2.3) is replaced by the integration for $r\geqslant R$. For the potential $\varphi(r)=A/r^n$ the contribution of external shells is $\Delta c_{11}=\Delta c_{33}\approx 2/v\int_R^\infty dr\int r^2 d\Omega\,\varphi''_{r^2}(r\,\sin\theta)^4$, where $\varphi''_{r^2}=(n+2)nA/(4r^{n+4})$, $d\Omega=d\phi d\theta\,\sin\theta$ and (r,ϕ,θ) are ordinary polar coordinates. The simple calculation gives

$$\Delta c_{11}^*=\Delta c_{11}=\frac{2}{5}\frac{\pi n(n+2)A}{(n-2)v^2R^{n-3}}. \tag{2.5}$$

Similarly,

$$\Delta c_{12}^*=\Delta c_{44}^*=\frac{2}{15}\frac{\pi n(n+2)A}{(n-2)v^2R^{n-3}}. \tag{2.6}$$

The correction for pressure from Eq. (2.4) has the same order:

$$\Delta P=\frac{2}{3}\frac{\pi nA}{(n-2)v^2R^{n-3}}. \tag{2.7}$$

Equations (2.5)–(2.7) are valid for strong enough potentials $(n>3)$. For the Lennard-Jones interaction these corrections decrease very rapidly with R. We used for the calculation $R=50a$ (a is the lattice constant). The results of calculation for the virtual Lennard-Jones solids are shown in Figs. 1 and 2. One can conclude, that the relative contribution from external atoms (all shells except for the first one) to the shear constants drops with pressure. In the case of bcc structure we should take into account the two nearest neighbors (Fig. 2). The reason is a relatively small value of the radii ratio between the second and first shells, $r_2/r_1=2/\sqrt{3}\approx 1.155$. The $c_{44}^*(P)$ dependence for sc structure asymptotically approximates (in logarithmic scale) the dependence $c_{44}^*(P)=-P$ existing for the model with nearest-neighbors interaction.[32] Similar behavior is observed for the positive constants in Fig. 1 and Fig. 2. It is necessary to emphasize, that the mentioned trends take place for logarithmic coordinates only and in a certain physically reasonable pressure interval. For linear scales the asymptotic relations are usually absent, but relative divergence decreases. The main reason for the trends mentioned above is the strong dependence of nearest-neighbor repulsion forces $\sim d^{12}$ (d is the nearest-neighbor distance, $d=r_1$). The equilibrium distance d_0 $(P=0)$ is usually very close to the minimum position of pair interaction function $\psi(r)$ but somewhat smaller. At the same time, the second and third coordination spheres are, as a rule, in the vicinity of the bend point of $\psi(r^2)$ and, thus, they give minor central contributions into the elastic constants (except for bcc). More distant atoms give a small negative contribution $(\psi''_{r^2}<0)$ into the shear constants and pressure.

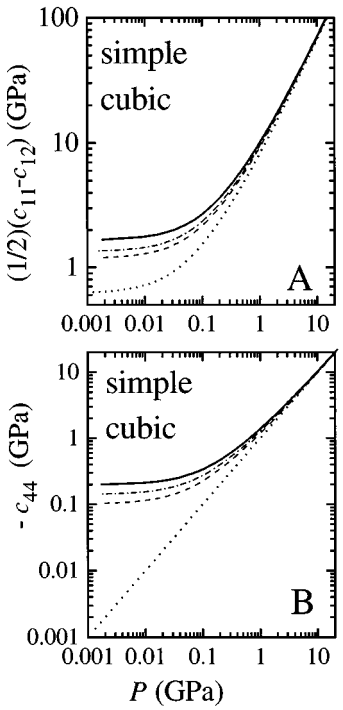

FIG. 1. Pressure dependence of $(1/2)(c_{11}-c_{12})$ constant (A) and c_{44} constant with inverse sign (B) for a simple cubic virtual structure of the Lennard-Jones particles with nearest neighbors (short dashed lines), with two (dashed), and with three (dashed and dotted) nearest-neighbor interactions. Solid lines correspond to the long-range interaction. Parameters of the potential ($\epsilon=3.1\times10^{-3}$ eV and $\sigma=2.74$ Å) are taken for Ne.

In real crystals the repulsion potentials $\psi(r)\sim 1/r^n$ have usually a strong distance dependence, $n\sim 8-12$. More accurate quantum-mechanic calculations and approximation of the experimental data have shown, that the Born-Mayer function $\psi(r)=B\exp(-r/\rho)$ is more adequate for description of the interatomic overlap forces.[26,33] Within the relatively narrow distance interval around the equilibrium distance d the Born-Mayer potential may be approximated using the dependence A^*/r^{n^*} with $n^*=-r\psi'/\psi=d/\rho$. The value of ρ varies within the interval 0.2–0.4 Å,[26,33] whereas $d\sim 2-4$ Å, i.e., $n^*\sim 10$.

The value of pressure increase at compression can be estimated [Eq. 2.4] from the asymptotic relation $P\sim 1/d^{n+3}$, where index n characterizes the repulsion potential $\sim 1/r^n$, and we take into account $v\sim d^3$. Thus, the negative contri-

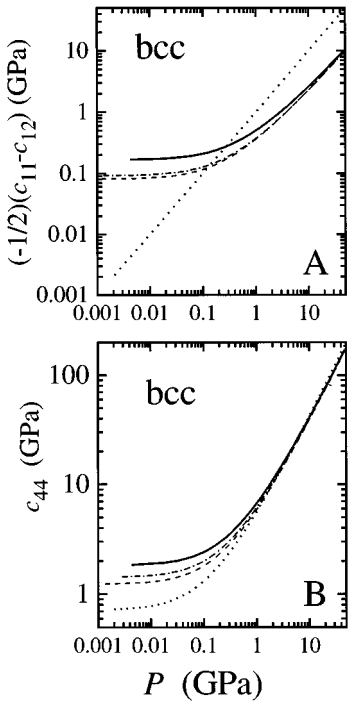

FIG. 2. Pressure dependence of $(1/2)(c_{11}-c_{12})$ constant with inverse sign (A) and c_{44} constant (B) for bcc virtual structure of the Lennard-Jones particles. The parameters of potential and notation are the same as in Fig. 1.

butions from the thermodynamic term $P\Delta V$ into elastic stiffness eigenconstants also strongly depend on the interatomic distance ($\sim 1/d^{n+3}$) [Eq. 2.3]. In close-packed lattices the nearest-neighbor repulsion plays a stabilizing role [$\psi''_{r^2}(d^2)>0$ and $\psi''_{r^2\sim 1/d^{n+4}}$], and the shear stiffness constants increase with pressure. Different forces are responsible for stability of real open-packed crystals with different kinds of bonding: the Madelung energy, or ion-ion interaction, in ionic substances ($u\sim 1/d$); the bond-bending forces in covalent crystals ($u\sim 1/d^2$); and the electron-ion Coulomb interaction ($u\sim 1/d$) and exchange potential ($u\sim 1/d$) in metals.[27] The positive contributions to shear eigenconstants from the energy terms mentioned above have a relatively weak dependence on the interatomic distance, $\sim 1/d^4$ or $\sim 1/d^5$. Thus, the elastic instability of sc (caused by c^*_{44}) and bcc [caused by $(1/2)(c^*_{11}-c^*_{12})$] lattices or their binary analogs ($B1$ and $B2$ structures) is inevitable under compression. (This conclusion is questionable in the case of bcc metals, where the quantum electronic effects are at work.)

An example of alkali halides allows us to illustrate quantitatively the competition between the destabilizing repulsive forces and the Madelung contribution. The rocksalt structure ($B1$) has a two-atomic elementary cell. During uniform deformation the internal displacement of atoms in the cell is zero, $\mathbf{u}(1)-\mathbf{u}(2)\equiv 0$. So, the static rocksalt structure is equivalent to a simple cubic one in the case of uniform deformation. But the Madelung energy $-\alpha e^2/d$ appears to be due to the long-range ion-ion interaction. We have tested the two empirical models from Ref. 26 (Chap. 1), that take into account the Madelung energy and the nearest-neighbor or the two-nearest-neighbor repulsion in the Born-Mayer form. For analysis of the stability criteria only the knowledge of c^*_{44} is of interest because the tetragonal shear stiffness constant $1/2(c^*_{11}-c^*_{12})$ increases with pressure. The calculation details and numerical results for certain alkali halides are presented in Appendix A and in Table I.

We can conclude, that a relatively simple calculation predicts the c^*_{44} instability and semiquantitatively describes the trends in high-pressure elastic behavior. It should be emphasized that the empirical potentials used here had been developed only for evaluation of the bulk modulus, interatomic distance, and cohesive energy, but they seem to describe correctly the main dynamic factors as well. From Table I one can see, that the estimated values of P_{inst} are usually higher than the pressures of phase transformations, which indicates the necessity for using more accurate potentials and, besides, for studying the low-temperature transformations in alkali halides under pressure. Similar calculation for ionic bcc crystals clearly show $(1/2)(c^*_{11}-c^*_{12})$ instability.

TABLE I. c^*_{44} elastic stiffness constant and its pressure derivative for alkali halides calculated from the first (M1) and the second (M2) models (Appendix A) in comparison with the experimental data. Instability pressures are evaluated for the condition $c^*_{44}=0$.

	Model 1		c^*_{44} (GPa)			$\partial c^*_{44}/\partial P$			P_{inst} (GPa)		
Compound	ρ (Å)[a]	λ[a] (10^{-16} J)	Expt.[b]	M1[c]	M2	Expt.[b]	M1	M2	M1	M2	P_{tr}[d] (GPa)
NaF	0.288	1.11	28.2	28.1	35.2	0.21	-0.21	0.62	50	330	27
NaCl	0.328	1.47	12.7	12.9	16.4	0.37	-0.27	0.47	21.6	241	29
NaBr	0.333	1.94	10.15	10.2	13.6	0.42	-0.31	0.53	16.6	10^4	29
KCl	0.324	3.63	6.3	8.19	8.95	-0.41	-0.38	-0.03	12.7	24.7	1.95
KBr	0.334	3.93	6.42	6.85	7.42	-0.30	-0.39	-0.06	10.5	20.2	1.75
KI	0.349	4.60	5.08	5.20	5.80	-0.23	-0.41	-0.04	7.86	18.0	1.75
RbCl	0.338	3.46	4.75	6.93	7.14	-0.60	-0.38	-0.13	10.7	6.8	0.52
RbBr	0.350	3.51	3.84	5.88	5.90	-0.56	-0.38	-0.19	9.1	12.8	0.42
RbI	0.352	5.80	2.79	4.47	4.60	-0.49	-0.43	-0.22	6.7	9.96	0.36

[a]Reference 26.
[b]Reference 34.
[c]See also Ref. 27.
[d]Reference 35.

Summarizing, in this section we have found from the generalized elastic stability criteria,[18] that the c_{44}^* instability of the sc and the $(1/2)(c_{11}^*-c_{12}^*)$ instability of bcc structures under compression result from the symmetry of lattice structure and are due to the strong nearest-neighbor repulsion. This conclusion will be supported by analysis of a diamondlike structure in the next section. But, in this case, features of the pressure-induced instability will be found.

III. LATTICE INSTABILITY OF TETRAHEDRAL SEMICONDUCTORS

A. Potential function

The stability of a diamondlike lattice ($Z=4$) is the sequence of noncentral forces that can be described in a first approximation by a three-body potential. The potential energy in this case may be presented as

$$U(\mathbf{X})=\sum_i \varphi_1(i)+\sum_{i<j} \varphi_2(i,j)+\sum_{i<j<k} \varphi_3(i,j,k), \tag{3.1}$$

where i, j, and k correspond to numbers of atoms. The simplest valence force field model[36] takes into account the bond-stretching $k_r\Delta r_{ij}^2/2$ and bond-bending $k_\theta\Delta\theta_{ijk}^2/2$ energies (Δr_{ij} and $\Delta\theta_{ijk}$ are deviations of bond length and interbond angle, respectively, from their equilibrium values).

Recently a series of different potentials has been developed to describe various physical properties of silicon and its non-diamond modifications and clusters.[37] But the analytical application of these potentials is practically impossible, and the appropriate choosing of their parameters for a wide range of IV-IV and III-V compounds is a very difficult task. For this reason we used a separable form of Eq. (3.1) with pair φ_2 and triplet φ_3 terms restricted by the nearest-neighbor interaction cutoff. Using a function of the Born-Mayer type is more adequate for description of the central overlap forces under high pressure. The Morse function is suitable for description of pair interaction

$$\varphi_2(i,j)\equiv\psi(r)=A_1\exp(-r/\rho)-A_2\exp(-r/2\rho), \tag{3.2}$$

where $r\equiv r_{ij}$. The general form of the three-body potential in the framework of the valence force field has been considered by Musgrave and Pople,[38] or, in a simplified version, by Martin[39]. The force constants in these potentials are fixed, that is not suitable for high-pressure applications. The indicated problem may be resolved by means of the constants depending on the interatomic distance. We used the universal Harrison's d^{-2} dependence[27] describing matrix elements between the overlapped states of hybridized electrons. We have preferred the simplest ''bond-bending'' form of a three-body potential:

$$\varphi_3(i,j,k)=\frac{1}{2}\,C_{\theta 0}\frac{d_0^2}{d^2}\,\Delta\theta_{ijk}^2, \tag{3.3}$$

where pair $i-j$ and pair $j-k$ ($i\neq k$) are the nearest neighbors and $\Delta\theta_{ijk}$ is the deviation of the angle between ij and jk bonds from its equilibrium value. [Further we will use the distance-depending parameter $C_\theta=C_{\theta 0}(d_0/d)^2$.] There are two reasons for such simplification. This potential is adequate for considering small strains in the diamond structure, if distortions of the tetrahedral SRO'S are not strong. Another reason is that the potential including pair and triple terms, according to Eqs. (3.2) and (3.3), describes the two main dynamic factors under compression—the central overlap forces and shear rigidity. The use of several force parameters allows us to correct the numerical results, but the contributions of these noncentral second-order terms have the same nature and should have approximately the same d^{-2} dependence as the bond-bending constant and, thus, they cannot significantly change the stability conditions.

The expressions obtained below may be easily adapted for the general case, taking into account the results of Martin[39] and Solbrig[40] for zero-pressure condition. We did not consider the Madelung energy for III-V compounds associated with a certain ionicity. This contribution is relatively small and has the weak distance dependence ($\sim d$). The corresponding correction of our results for zinc-blende semiconductors may be performed using the calculation of Ref. 39. One can note that a partial ionicity reduces the stability of a diamond structure, which may be approximated by the decrease of a bond-bending force constant.

The constant $C_{\theta 0}\equiv C_\theta(0)$ has been chosen to approximate the $(1/2)(c_{11}-c_{12})$ modulus. The parameters of the Morse potential have been derived from the lattice constant, bulk modulus, and its pressure derivative. (See Appendix B 1 and Table II.) We have used for the input data the isoentropic modulus measured near room temperature because this value differs from the zero-temperature evaluation by less than 5%.[41] We have also executed calculations with the generalized Morse potential having the attraction radius $\rho_2\neq 2\rho$ [Eq. (3.2)], which allows us to approximate cohesive energy. In this case, the numerical results were the same to an accuracy of about 1%.

Unfortunately, we cannot use the values of $C_{\theta 0}$ describing a simple shift $(\epsilon,-\epsilon,0)$ for the analysis of the Brillouin-zone boundary (BZB) phonons. According to Harrison,[27] the evaluation of $C_{\theta 0}$ based on the frequencies of BZB modes gives values 2–3 fold less, which corresponds to a flattening of TA branches near the BZB. This discrepancy is associated with long-range electron correlation effects[27] and may be described in the framework of the Weber bond charges model.[42] In the valence force field model of Solbrig[40] this difference is mainly defined by the second-order constant corresponding to the two angles between three subsequent planar bonds in the plane [1,1,0] or equivalent (coplanar angle-angle interaction). (See also Ref. 43.) We use another approach introducing a bond-bending constant $C_\theta(\mathbf{k})$ depending on $\mathbf{k}$-wave vector and approximating room-pressure data. One should note, that the bond-stretching constants k_r evaluated from elastic properties and from frequencies of the BZB phonons are very close[27] and, therefore, we have used the same pair potential in both cases.

B. Elastic instability

In the framework of the potential described by Eqs. (3.1)-(3.3) the stiffness elastic constants defining the shear stability of a diamond structure are written in the following form (see Appendix B 2):

TABLE II. The input experimental data, parameters of the Morse potential, the bond-bending force constant, and certain calculated elastic properties for IV-IV and III-V compounds. The corresponding experimental data are presented in parentheses for comparison (Ref. 41).

Properties	C	Si	Ge	GaP	GaAs	GaSb	InP	InSb
$a=d\sqrt{3}/4$ (Å)	3.567	5.431	5.658	5.451	5.653	6.096	5.869	6.479
B (GPa)	442	97.3	75.0	88.8	75.4	56.35	71.0	45.7
B_P'	4.05	4.24	4.41	4.79	4.49	4.75	4.59	4.90
$(1/2)(C_{11}-c_{12})$ (GPa)	475.6	50.9	40.1	39.3	32.5	24.0	22.3	15.15
ρ (Å)	0.2531	0.3629	0.3592	0.3113	0.3519	0.3520	0.3539	0.3597
A_1 (eV)	1690	1701	1881	3444	2113	2885	2570	3509
A_2 (eV)	160.1	133.3	124.3	155.6	128.9	135.7	141.8	142.05
$C_{\theta 0}(\epsilon,-\epsilon,0)$ (eV)	8.43	3.19	2.84	2.49	2.295	2.13	1.76	1.61
c_{44}^* (GPa)	490	69.9	54.7	56.8	47.3	35.1	35.1	23.6
	(577)	(79.6)	(66.8)	(70.5)	(59.4)	(43.2)	(46.0)	(30.0)
dc_{11}^*/dP	5.11	4.07	4.27	4.44	4.12	4.36	3.96	4.30
	(6.0)	(4.33)	(5.03)	(4.77)	(4.63)	(4.96)	(4.17)	(4.75)
dc_{12}^*/dP	3.52	4.33	4.48	4.96	4.68	4.94	4.91	5.20
	(3.1)	(4.19)	(4.31)	(4.79)	(4.42)	(4.64)	(4.80)	(4.97)
dc_{44}^*/dP	1.87	0.42	0.51	0.23	0.13	0.15	-0.36	-0.24
	(3.0)	(0.80)	(1.41)	(0.92)	(1.10)	(1.01)	(0.36)	(0.53)

$$\frac{1}{2}(c_{11}^*-c_{12}^*)=\frac{3\sqrt{3}C_\theta}{4d^3}+\frac{\sqrt{3}\psi'_{r^2}(d^2)}{2d}, \tag{3.4a}$$

$$c_{44}^*=\frac{\sqrt{3}}{d}\left[\frac{\psi'_{r^2}(\psi''_{r^2}r^2+C_\theta/2r^2)+3C_\theta\psi''_{r^2}}{3\psi'_{r^2}+2\psi''_{r^2}r^2+4C_\theta/r^2}\right]_{r^2=d^2}+\frac{\sqrt{3}\psi'_{r^2}(d^2)}{2d}, \tag{3.4b}$$

where ψ is the pair potential and as usual $\psi'_{r^2}(d^2)=\psi'_r(d)/2d$, etc. The equilibrium condition for a diamond structure is given by the equation (Appendix B 2):

$$P=-\frac{\sqrt{3}\psi'_{r^2}(d^2)}{2d}. \tag{3.5}$$

To test the potential we have calculated pressure derivatives of the stiffness elastic constants and c_{44}^* modulus. The data obtained are compared with the experiment in Table II for certain IV-IV and III-V compounds. It is evident that the constants c_{11} and c_{12} are approximated exactly in the framework of the current potential. It is shown that our model appropriately describes the main trends in the elastic properties of tetrahedral semiconductors. Nevertheless, the values of c_{44}^* which fit into Harrison's calculation in the framework of the room-pressure valence force field model,[27] and the pressure derivatives of c_{44}^* and $(1/2)(c_{11}^*-c_{12}^*)$ are somewhat underestimated. The current numerical calculations may be improved using a stronger distance dependence for the bond-bending constant $C_\theta(d)$. On the other hand, C_θ is proportional to the degree of covalency,[27] which decreases under pressure due to a dehybridization of the valence states. A proper function may be chosen in the form $C_\theta(d)=C_{\theta 0}(d_0/d)^n(\alpha_c(d)/\alpha_{c0})$, where the function $\alpha_c(d)$ approximates the degree of covalency. Higher values for n ($n\sim 3$–4) allow us to get better numerical results at room pressure. More general approach is to take into account other second-order terms,[38,40] second-neighbor interaction,[36] and the Coulomb energy for binary compounds,[39] but this is outside the scope of the present paper.

The evaluated instability pressures P_{inst}, corresponding to the shear stability criteria from Eq. (2.1), are presented in Table III. The $(1/2)(c_{11}^*-c_{12}^*)$ instability has the same geometrical origin as the shear instability of bcc structure. Nearest neighbors in diamond together with points inverted around the central atom correspond to the first coordination sphere of the bcc structure. The tetragonal shear deformation does not lead to the internal strain in a cell. On the contrary, c_{44}^* instability appears to be due to the internal strain. This is another type of instability. According to Eq. (3.4b), the positive contribution of central repulsion $[\sim\psi''_{r^2}(d^2)]$ to c_{44}^* asymptotically disappears during compression, whereas this term is totally absent in the case of the $(1/2)(c_{11}^*-c_{12}^*)$ constant. In both cases, the central repulsive forces play a dominant role in the vanishing of shear stiffness eigenconstants, which is in accordance with the conclusion of the previous section.

It is interesting to compare our results with the recent application of generalized stability criteria to the Tersoff potential in silicon.[45] In the last work the critical pressures for tetragonal and rhombohedral instability at zero temperature are equal to 105 and 114 GPa, respectively. Our predictions for Si (Table III) are very close to these values, but the order of critical pressures is reverse. Such a difference seems to be due to the uncertainty in choosing an adequate atomic potential. Extrapolation of the experimental ultrasonic data for Si gives the critical pressures 40 and 78 GPa for c_{44}^* and $(1/2)(c_{11}^*-c_{12}^*)$ instabilities, respectively.[32]

C. Vibration instability

The elastic stability criteria are insufficient for consideration of the pressure-induced lattice collapse. The whole

TABLE III. The pressures of absolute instability P_{inst} for some IV-IV and III-V compounds, corresponding to different conditions, the recalculated pressures P^*_{inst} for d^{-n} scaling of $C_{\theta 0}$ [$n(X)\approx 4.29$ and $n(L)\approx 3.66$], and the pressures of phase transition at room temperature (Ref. 35).

	P_{inst} (GPa)				P^*_{inst} (GPa)		
	$(c^*_{11}-c^*_{12}=0)$	$(c^*_{44}=0)$	$(\nu_{TA(X)}=0)$	$(\nu_{TA(L)}=0)$	$(\nu_{TA(X)}=0)$	$(\nu_{TA(L)}=0)$	P_{tr} (GPa)
Si	108	105	23	28	27	32	12
Ge	84	82	15	20	18	23	9.5
GaP	71	70	19	28	23	34	21.5
GaAs	60	58	15	19	17	22	16.6[a]
GaSb	43	42	9.2	12.5	10.5	14	7.5
InP	35	34.6	10.6	14	12	16	8–9.7
InSb	24	23.6	4.3	7.0	4.7	7.6	2.6
BAs[b]	230	221	61	75	87	100	125[c]

[a]Reference 44.
[b]The constants $C_{\theta 0}(X)$ and $C_{\theta 0}(L)$ are evaluated from the intercompound $C_{\theta 0}(d_0)$ dependences.
[c]Reference 24.

phonon spectrum of a crystal and vibration eigenmodes should be taken into account in the general case.

The softening of TA modes on the BZB under pressure and negative values of the Grüneisen constants for these modes are well known for tetrahedral semiconductors both from experiments[46] and *ab initio* calculations[47]. In Ref. 47 it was shown that the role of noncentral stabilizing forces diminishes under compression because the system becomes more metallic. Our model allows us to obtain direct expressions for the phonon frequencies in high-symmetry points. (See Appendix B 3.) The numerical calculation indicates that the BZB phonon modes, except transverse-acoustic phonons, stiffen under pressure. This is in accordance with the experimental signs of the Grüneisen constants (Table IV). In the case of ordinary IV group semiconductors ($M_1=M_2=M$) the equations for frequencies of the TA(X) and TA(L) modes are simplified:

$$\omega^2_{TA}(X)=2\omega^2_{TA}(L)=\frac{1}{M}\left(12\frac{C_\theta}{d^2}+8\psi'_{r2}(d^2)\right). \quad (3.6)$$

Equation (3.6) has the same structure as Eq. (3.4a) for $(1/2)(c^*_{11}-c^*_{12})$, which demonstrates the competition between the stabilizing noncentral term and the pair repulsive interaction. [$\psi'_{r2}(d^2)$ is negative at $P>0$ and proportional to pressure.]

In most cases, the numerical calculation gives good results for the phonon frequencies and certain Grüneisen constants (Table IV). When $C_\theta(\epsilon,-\epsilon,0)$ is used, $\sim$10–20 % overestimation is observed for Γ-optic phonons. (These data are not important for the stability study and are not presented here.) Thus, the presented simplified calculation correctly takes into account the main dynamic factors determining the vibration properties. The frequency of the LA(L) mode depends only on the central potential, and the evaluated data for $\omega_{TA}(L)$ are excellent. The negative Grüneisen constants for TA(X) phonons are $\sim$1.5 times overestimated in their magnitudes. Therefore, the instability pressures estimated for the condition $\omega_{TA}(X)=0$ in Table III should be increased by approximately one and a half. (One should note that the value ω^2_{TA} approximately linearly decreases with pressure.)

The use of d^{-n} scaling for the bond-bending potential in Eq. (3.3) gives better results for the Grüneisen constants of TA modes (Table IV), if n approximates d^{-n} scaling of the distance dependence $C_{\theta 0}(d_0)$, corresponding to various compounds. In this case the positive Grüneisen constant of the TA(X) mode for carbon becomes predictable. The development of a more accurate high-pressure valence force potential based, for example, on the room- pressure potential of Kane,[43] is a prospect for a future study.

From Table III it is clear that the pressure-induced collapse of a thermally frozen diamond structure should be driven by the TA(X) mode, which is supported by the evaluation of the TA($\Gamma-X$) branch under high pressure. (See Appendix B 4 and Fig. 3.) The TA(X) instability appears, when the elastic softening, connected with c^*_{44} for $\Gamma-X$ branch, is practically absent. Comparison with the experiment[46] indicates the necessity to scale the pressures in Fig. 3 by a factor $\gamma_{calc}/\gamma_{exp}$ as mentioned above. Nevertheless, the character of the high-pressure behavior of the TA ($\Gamma-X$) branch remains the same. Thus, the BZB phonon instability occurs at pressure $\sim$1.5–2 times higher than the pressure of the equilibrium transition and $\sim$2–4 times less than the pressure of elastic instability.

It is interesting to evaluate the instability pressure for zinc-blende BAs because disordering of this compound has been observed under compression even at room temperature.[24] Unfortunately, we have no experimental data for the phonon frequencies and elastic constants in BAs. To approximate the $C_{\theta 0}(X)$ and $C_{\theta 0}(L)$ model constants we have used the d^{-n} fitting of $C_{\theta 0}(d_0)$ distance dependence for other semiconductors (Table IV). The calculated instability pressure for BAs (Table III) is two times less than the amorphization pressure $P_{am}=125$ GPa (Ref. 24) and so, seems to be underestimated. In any case, this is the satisfactory correspondence, if we take into account the rough character of the approximation for $C_{\theta 0}$ and systematic underestimation of P_{inst} in our calculation.

IV. DISCUSSION

A. Symmetry of instability and solid-state amorphization

Whereas the stability criteria allow us to predict the onset of structural collapse, the rules determining the final struc-

TABLE IV. The bond-bending constants for X and L point with experimental input frequencies, calculated X- and L-mode frequencies, and Grüneisen constants for IV-IV and III-V compounds. The experimental data (Refs. 41) are also presented in parentheses or follow behind the slash, if known. The parameters $\gamma^*_{TA}(X)$ and $\gamma^*_{TA}(L)$ correspond to the recalculation with d^{-n} scaling of $C_{\theta 0}$ using $n(X)\approx 4.29$ and $n(L)\approx 3.66$, that have been obtained from fitting of the $C_{\theta 0}(d_0)$ dependence for various compounds.

Properties	C	Si	Ge	GaP	GaAs	GaSb	InP	InSb
$\nu^{(exp)}_{TA}(X)$ (THz)	24.2	4.49	2.38	3.13	2.36	1.70	2.05	1.12
$\nu^{(exp)}_{TA}(L)$ (THz)	16.9	3.43	1.87	2.58	1.86	1.37	1.65	0.98
$C_{\theta 0}(X)$ (eV)	5.73	1.069	0.842	0.945	0.819	0.658	0.686	0.396
$C_{\theta 0}(L)$ (eV)	5.59	1.248	1.039	1.277	1.018	0.852	0.881	0.607
$\nu_{LA}(X)$ (THz)	38.2	11.8	6.5	7.11	6.4	4.5	5.0	4.04
	(35.5)	(12.3)	(7.14)	(7.46)	(6.80)	(4.99)	(5.8)	(4.30)
$\nu_{LO}(X)$ (THz)	38.2	11.8	6.5	10.7	6.6	5.9	9.7	4.16
	(35.5)	(12.3)	(7.14)	(10.65)	(7.22)	(6.36)	(9.70)	(4.75)
$\nu_{TO}(X)$ (THz)	41.0	15.3	8.5	11.9	8.6	6.9	10.4	5.56
	(32.0)	(13.9)	(8.17)	(11.0)	(7.56)	(6.35)	(9.95)	(5.38)
$\nu_{LA}(L)$ (THz)	34.8	10.0	5.5	6.8	5.5	4.1	4.7	3.33
	(30.2)	(11.35)	(6.63)	(6.45)	(6.26)	(4.61)	(5.00)	(3.81)
$\nu_{LO}(L)$ (THz)	37.8	13.2	7.34	11.0	7.38	6.19	9.87	4.81
	(37.5)	(12.6)	(7.27)	(10.64)	(7.15)	(6.15)	(9.50)	(4.82)
$\nu_{TO}(L)$ (THz)	46.4	15.9	8.9	12.4	8.9	7.2	10.7	5.7
	(36.2)	(14.68)	(8.55)	(11.24)	(7.84)	(6.48)	(10.2)	(5.31)
$\gamma_{TA}(X)$, calc/exp	0.0/0.4	-2.2/-1.4	-2.5/-1.53	-2.3/-0.72	-2.6/-1.62	-3.1	-3.3/-2.1	-5.5
$\gamma^*_{TA}(X)$	0.37	-1.8	-2.1	-1.9	-2.2	-2.7	-2.9	-5.0
$\gamma_{LA,LO}(X)$, calc/exp	0.82	1.06/0.9	1.1	1.2/1.0	1.2	1.3	1.2	1.4
$\gamma_{TO}(X)$, calc/exp	1.4/2.0	1.5/1.5	1.6	1.7/1.3	1.7/1.73	1.8	1.6/1.4	1.9
$\gamma_{TA}(X)$, calc/exp	0.0	-1.8/-1.3	-1.9/-0.4	-1.5/-0.8	-2.0/-1.7	-2.2	-2.5/-2.0	-3.3
$\gamma^*_{TA}(L)$	0.24	-1.5	-1.6	-1.2	-1.7	-2.0	-2.2	-3.0
$\gamma_{LA}(L)$, calc/exp	0.5	0.45/0.9	0.5/0.5	0.9	0.5	0.7	0.85	0.6
$\gamma_{LO}(L)$, calc/exp	1.5/1.3	1.6/0.9	1.7/1.2	1.6	1.7	1.7	1.5	1.9
$\gamma_{TO}(L)$, calc/exp	1.2/1.4	1.35/1.3	1.4/0.9	1.56/1.5	1.5/1.48	1.6	1.47/1.4(2)	1.7

ture of a solid after a transition are not well understood. Most alkali-halides transit under pressure to the $B2$ structure.[35] The $B1 \rightarrow B2$ transformation corresponds to rhombohedral deformation, i.e., it should be driven by the c^*_{44} softening.[48]

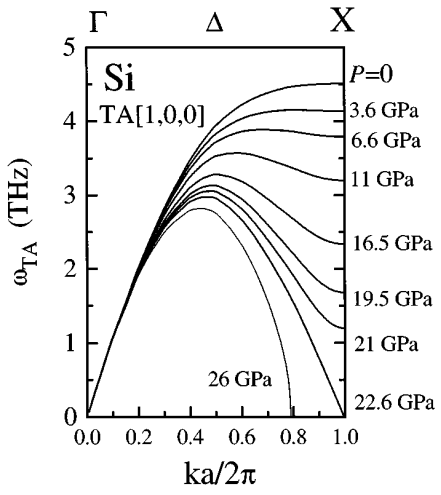

FIG. 3. Evolution of the transverse-acoustic branch for [1,0,0] direction under high pressure. Comparison of the calculation with the experiment indicates the necessity of pressure scaling by factor ~ 1.5.

Ionic solids in a CsCl phase ($B2$) transform to a tetragonal phase under high pressure, and this transition is driven by the $(1/2)(c^*_{11}-c^*_{12})$ softening.[49] Correspondence between the symmetry of a soft mode (Sec. II) and the type of a phase transition observed appears to be not an accidental circumstance. The recent molecular-dynamics calculation[18] has given the close agreement between the predicted and observed symmetry characteristics of the first instability. At the thermodynamic extremity (high temperatures) any phase transition comes to an equilibrium state. At low temperatures a transformation in a solid, triggered by instability, follows the paths with minimal energy barriers and may have the finish in nonequilibrium metastable states, including disordered. The β-tin Si II and Ge II phases may serve as a striking experimental example illustrating the driving role of temperature for nonequilibrium transformations.[6] During relatively fast decompression, when temperature decreases, the high-pressure modifications undergo a number of transitions: Si II $\rightarrow$ Si I, Si II $\rightarrow$ Si III (BC-8), and Si II $\rightarrow$ a-Si in silicon and Ge II $\rightarrow$ Ge I, Ge II $\rightarrow$ Ge III (ST-12), Ge II $\rightarrow$ Ge IV (BC-8), and Ge II $\rightarrow$ a-Ge in germanium.

When the symmetry of instability is in close crystallographic relation with the transition to a thermodynamically equilibrium state, a martensitic crystal-crystal transition may be expected under instability conditions. For example, the

$B1 \rightarrow B2$ transition is martensitic and usually has a narrow hysteresis. For KCl this hysteresis is small down to helium temperatures.[50] A lot of metals have martensitic fcc$\leftrightarrow$bcc transitions at low temperatures,[35] which are caused by the shear elastic softening. This indicates, that the correspondence between elastic instability and amorphization is not evident and trivial. Indeed, a vanishing of an elastic eigenconstant is associated with the phonon softening in a long-wave limit $\mathbf{k} \rightarrow 0$. In this case, coherent oscillations for $\mathbf{k} \rightarrow 0$ should lead to a martensitic crystal grain-crystal grain transformation in a large region, i.e., to an activationless crystal-crystal transition instead of amorphization.

The symmetry origin of the SSA may be clarified from the results of the previous section. A diamondlike crystal with atoms dislaced in the TA(X) mode has to be treated as an orthorhombic structure (point group mm).[51] The usual high-pressure phases of tetrahedral semiconductors have β-tin or NaCl-like structures. The exception is gallium arsenic transforming the orthorhombic high-pressure phase GaAs(II) with the space group $Pmm2$.[44] We cannot rule out the possibility, that the GaAs(II) phase may be obtained by the ''martensitic'' TA(X) softening. The β-tin structure corresponds to the tetragonal $(\epsilon, \epsilon, -2\epsilon)$ deformation of a diamond lattice. The corresponding transition has to be driven by the $(1/2)(c_{11}^* - c_{12}^*)$ instability, which is supported by the recent molecular-dynamics calculation for silicon with the Tersoff potential.[45] The NaCl structure may be obtained by the relative shift of the fcc sublattice in the [1,1,1] direction, which is connected with the softening of Γ-optic phonons. From the numerial analysis of different stability criteria we can suppose, that the SSA of some IV-IV and III-V semiconductors (probably except for GaAs) may be actually observed under compression, if a crystal is thermally frozen, because the mode triggering instability [TA(X)] does not coincide with the path to a high-pressure phase. At low temperatures the existence of an activation barrier against homogeneous deformation[45] prevents the ordinary first-order crystal-crystal transition.

There are additional crystallographic arguments. The TA (X) phonons in diamond structure have six independent modes with the nonequivalent symmetry of perturbed states of a lattice, which may destroy the coherent scenario of a structural transition. At the same time the TA(L) instability occurs at very close pressures and must significantly affect the real kinetics of a structural collapse. The atomic size effect in the pressure-induced amorphization of a binary covalent lattice[25] seems also to be very important.

The volume drop in tetrahedral semiconductors during the transition is about 15–22 %.[35] This experimental fact supports the supposition about the possibility of a low-temperature SSA in diamondlike crystals. Great stresses, $\sigma \sim G\Delta V/V$, arising during the transition prevent a structurally coherent crystallite-crystallite transformation in an extensive region. Futher studies are needed to clear up this problem.

B. Geometrical origins of soft modes

The softening of elastic and phonon modes is well known in the literature for the instabilities, considered in the present paper. Our calculations shows that the ''mechanical'' origin

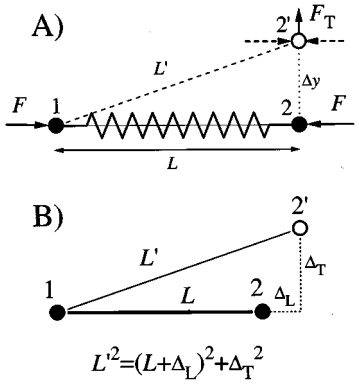

FIG. 4. The transverse displacement of the one end of compressed spring (A) or bond (B) leads to the linear-dependent transverse force in respect to the displacement (Δy or Δ_T) and only to a second-order length change.

connected with the strong nearest-neighbor overlap lies in the base of absolute instabilities driven by these modes. The mechanical nature of lattice softening under pressurizing is in close relation with ''the effect of a compressed spring.'' If a spring is compressed by a force F [Fig. 4(A)] a transverse displacement of its end leads to the second-order length change, $\Delta L \approx \Delta y^2/L$, whereas the transverse force appearing is linear with respect to the displacement $F_T \approx F\Delta y/L$. In the more general case of a two-body system (of a bond) with the central interaction $\psi(r)$ [Fig. 4(B)] the change of pair potential energy may be written up to the second-order term in a convenient form using the Taylor series for ψ as a function of r^2:

$$\Delta\psi = \psi'_{r^2}(2\Delta_L L + \Delta_L^2 + \Delta_T^2) + 2\psi''_{r^2}\Delta_L^2 L^2, \qquad (4.1)$$

where L is the bond length; Δ_L and Δ_T are the longitudinal and transverse components of relative displacement, respectively. When a bond is compressed, i.e., $\psi'_{r^2} < 0$, and $\Delta_L \equiv 0$ the change of energy $\Delta\psi = \psi'_{r^2}\Delta_T^2$ is always negative. In a crystalline lattice this effect tends to destabilize the system.

The appearance of terms ψ'_{r^2} in Eqs. (3.4) and (3.6) is due to this ''mechanical'' effect. The account of the term ψ'_{r^2}, which is proportional or asymptotically proportional to pressure, distinguishes our calculation from the preceding analytical valence force field studies. The stronger distance dependence of repulsive central forces between the nearest neighbors arises due to the overlap of core electrons. The quantum-mechanical origin of the central character of the overlap forces is closely connected with the central symmetry of core states. The role of competition between the short-range covalent and central repulsive interactions in the chemical trends of structural properties has been recently recognized for sp solids through the total-energy-minimization calculation.[52] Here we can see the role of this competition in the dynamic properties.

It is easy to see that the relative displacements of nearest neighbors are perpendicular to the bonds for elastic soft modes and lead only to the second-order changes in the bond length. For the c_{44} softening in diamond structure this state-

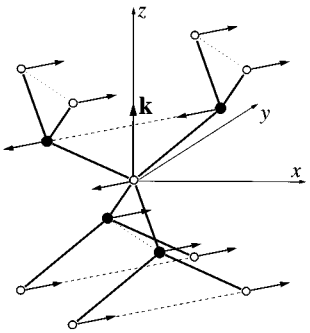

FIG. 5. The atomic displacements in TA(X) mode with wave vector $\mathbf{k}=(0,0,2\pi/a)$ and [1,1,0] polarization. The dotted lines correspond to the [1,1,0] direction.

ment is ''asymptotically'' valid. The unstable phonon modes on the BZB have atomic displacements perpendicular to the bonds too (see Fig. 5).

Thus, the application of elastic and vibration stability criteria to open-packed lattices under hydrostatic compression allows us to derive geometrical criteria for soft modes. The appearance of the c_{44} instability in a diamond structure is associated with the internal strain in an elementary cell. Clearly, the more complex is the structure of a crystal, the greater number of instability criteria, which may be satisfied, should exist. The principal distinction of expansion at $T=0$ is the possible bulk decohesive instability.[18,32] Under compression the bulk instability, corresponding to the finite volume discontinuity, seems to be possible only as a consequence of shear instability.

The problem of lattice instability on decompression of high-pressure phases[6,2] requires a special study. In this case, noncentral forces may give a negative contribution to shear eigenconstants, and usually the high-pressure modifications are metals. The role of temperature is extremely important for the experimental observation in this case because at $T=0$ the absolute instability pressures are often extrapolated to negative values [Si II, Ge II,[6] and GaSb II (Ref. 2)].

As to the role of temperature in the lattice instability, the importance of anharmonic effects at positive temperatures[53] should be noted. For a quantum system at zero temperature the lattice becomes unstable, if the zero-point energy per atom is comparable with the energy of a bond.[54] Some results clearing the problem may be found in Refs. 18, 25, and 32.

V. CONCLUSION

In the present paper we have considered the lattice instability as a driving force of the high-pressure SSA that allows us to restrict the analysis within the limits of a classical static lattice ($T=0$). The use of semiempirical potentials for molecular, ionic, and covalent crystals have allowed us to show, that the lattice instability on compression of a quantum system, such as a solid, may be understood in the framework of simple mechanical and geometrical concepts. We have shown that the pair repulsive interaction of nearest neighbors plays the central role in the problem of instability of a compressed open-packed crystal. The common feature of all instability types considered here [$(1/2)(c_{11}^*-c_{12}^*)$ in the bcc structure; c_{44}^* in NaCl; $(1/2)(c_{11}^*-c_{12}^*)$, c_{44}^* TA(X), and TA(L) in the diamond structure] is the competition between the destabilizing nearest-neighbor repulsion and the weaker stabilizing noncentral covalent or Madelung forces. The relative displacements of nearest neighbors in the soft modes are perpendicular or asymptotically perpendicular to the bonds, which gives a geometrical criterion for soft eigenmodes in complex structures. The structures with more than one atom per elementary cell may have soft modes connected with the internal strains in an elementary cell, which have been illustrated on the diamondlike structure. Our modeling gives a powerful method for analyzing the high-pressure lattice dynamics using the room-pressure potentials previously developed. New prospects for the dynamic analysis of complex structures are opened by combining the tight-binding approximation[52] with the mechanical approach presented here.

The calculations of high-pressure lattice dynamics for diamond and zinc-blende semiconductors has been based on generalization of the usual valence force field model. The basic feature of our approach is introduction of the general form (in particular, of the Morse type) of pair potential, taking into account the anharmonic nature of overlap forces, and distance scaling of the second-order force parameters. We have preferred the simplest bond-bending form of a three-body potential that allowed us to carry out the analytical calculation and obtain the reasonable quantitative results. The multiparameter fitting has been replaced by the **k**-vector dependence of a bond-bending constant. This allowed us to calculate the evolution of a phonon spectrum under high pressure using the experimental room-pressure data as the input. According to our calculation, the absolute instability of tetrahedral semiconductors should be governed by the TA (X) phonon softening. The supposition about the possibility of the SSA in pressurized tetrahedral semiconductors[3] is supported by crystallographic and kinetic arguments.

ACKNOWLEDGMENTS

The work was financially supported by the International Science Foundation (Grant No. MTK 300) and the Russian Science Foundation (Grant No. 95-02–03677).

APPENDIX A: ELASTIC PROPERTIES OF ALKALI HALIDES UNDER HIGH PRESSURE

The potential energy for the first model (nearest-neighbor repulsion) is written per pair of atoms as[26]

$$u(d)=-\frac{\alpha e^2}{d}+Z\lambda_{+-}\exp\left(-\frac{d}{\rho}\right). \tag{A1}$$

The constants ρ and λ_{+-} are given in Table I, the Madelung constant α for the rocksalt structure is approximately equal to 1.748, and $Z=6$. In the second model[26] the Born-Mayer function,

$$\varphi_{AB}(r)=\beta_{AB}b\exp\left(\frac{r_A+r_B-r}{\rho}\right),$$

describes the short-range repulsion between first-nearest neighbors and second-nearest neighbors (A and B indicate +

or − ion). In this case parameters $\rho=0.3333$ Å and $b=10^{-19}$ J are universal for all I-VII compounds; $\beta_{++}=1.25$, $\beta_{+-}=1.0$, and $\beta_{--}=0.75$. The constant r_A and r_B represent ionic radii (for Na^+ $r_+=0.94$ Å, K^+-1.235 Å, and Rb^+-1.37 Å; for F^- $r_-=1.05$ Å, Cl^--1.435 Å, Br^--1.56 Å, and I^--1.75 Å).

It is obvious that the first model is a particular case of model 2 (in this case $\beta_{++}=\beta_{--}=0$, i.e., $\varphi_{++}\equiv 0$ and $\varphi_{--}\equiv 0$). For this reason, we present the common expressions for both models. The pressure dependence versus distance may be determined as a volume derivative of energy:

$$P(d)=-\frac{\alpha e^2}{6d^4}-\frac{1}{d^2}\left[\frac{\partial\varphi_{+-}}{\partial r}(d)+\sqrt{2}\left(\frac{\partial\varphi_{++}}{\partial r}(\sqrt{2}d)+\frac{\partial\varphi_{--}}{\partial r}(\sqrt{2}d)\right)\right], \tag{A2}$$

where

$$\frac{\partial\varphi_{AB}}{\partial r}(r)=\frac{(-\beta_{AB}b)}{\rho}\exp\left(\frac{r_A+r_B-r}{\rho}\right).$$

The contribution of the Coulomb ion-ion interaction to c_{44} has been calculated by Kellermann:[55] $\Delta c_{44}^{ii}=\alpha_{44}e^2/d^4$, where $\alpha_{44}\approx 0.348$ for the NaCl structure. Using Eq. (2.3b) for the short-range repulsive interaction we obtain

$$c_{44}^*=\alpha_{44}\frac{e^2}{d^4}+4d\left(\frac{\partial^2\varphi_{++}}{\partial(r^2)^2}(2d^2)+\frac{\partial^2\varphi_{--}}{\partial(r^2)^2}(2d^2)\right)-P(d), \tag{A3}$$

where

$$\frac{\partial^2\varphi_{AB}}{\partial(r^2)^2}(r)=\frac{\beta_{AB}b}{4\rho r^3}\left(1+\frac{r}{\rho}\right)\exp\left(\frac{r_A+r_B-r}{\rho}\right).$$

Some elastic properties calculated according to Eqs. (A2) and (A3), as well as instability pressures ($c_{44}^*=0$) are compared in Table I with the experimental data. One should note, that the ultrasonic measurements under high pressure cited in Ref. 34 give isoentropic effective elastic constants which are very close to stiffness constants in solids.

It is well known[27] that the first model gives good evaluation for the room-pressure rhombohedral shear constant $c_{44}=c_{44}^*(0)=\alpha_{44}e^2/d^4$. Nevertheless, the second model is more adequate for prediction of $\partial c_{44}^*/\partial P(0)$ for the Na-VII set, since these salts have a small ratio of ionic radii r_+/r_- and the second-neighbor interaction is of great importance. The first model gives better predictions for the K-VII and Rb-VII sets.

APPENDIX B: ELASTIC AND DYNAMIC PROPERTIES OF THE DIAMOND STRUCTURE UNDER HIGH PRESSURE

The presented calculation are carried out for the potential Eqs. (3.1)–(3.3) from Sec. III ($\varphi_1\equiv 0$).

1. Parameters of the Morse potential

In the framework of current potential the bulk modulus and its pressure derivative depend only on the central forces ($T=0$):

$$B=[\sqrt{3}/12d^2)[d\psi''(d)-2\psi'(d)], \tag{B1}$$

$$B'(P)=\frac{-d^2\psi'''(d)+3d\psi''(d)-4\psi'(d)}{3[d\psi''(d)-2\psi'(d)]}, \tag{B2}$$

where ψ', ψ'', and ψ''' are ordinary distance derivatives. Using the equilibrium condition for lattice constant ($a_0=4d_0/\sqrt{3}$) at zero pressure, $\psi'(d_0)=0$, we can easily find from Eqs. (B1) and (B2) and from the definitive Eq. (3.2) the expressions for parameters of the Morse potential based on lattice characteristics:

$$\rho=\frac{d_0}{2(B_0'-1)},\quad A_1=8\sqrt{3}B_0d_0\rho^2\exp(d_0/\rho),$$

$$A_2=16\sqrt{3}B_0d_0\rho^2\exp(d_0/2\rho). \tag{B3}$$

2. Elastic constants

The full elastic Gibbs free energy of the uniformly deformed diamond structure may be presented in terms of the deformation tensor u_i ($i=1,\ldots,6$) and the internal strain (or relative displacement) $\Delta\mathbf{u}=\mathbf{u}(2)-\mathbf{u}(1)$ as follows:

$$\frac{\Delta G}{V}=D\sum_{i=1}^{3}u_i+\frac{Q}{2}|\Delta\mathbf{u}|^2+R(\Delta u_x u_4+\Delta u_y u_5+\Delta u_z u_6)+\frac{1}{2}\sum_{i,j}c_{ij}'u_iu_j, \tag{B4}$$

where

$$D=\sqrt{3}\psi_{r^2}'(d^2)/2d+P(d),$$

$$Q=\frac{3\sqrt{3}}{2d^3}\left(\psi_{r^2}'(d^2)+\frac{2}{3}\psi_{r^2}''(d^2)d^2+\frac{4}{3}\frac{C_\theta}{d^2}\right),$$

$$R=2[\psi_{r^2}''(d^2)-C_\theta/d^4]. \tag{B5}$$

The effective stiffness constants c_{ij}' have a cubic symmetry and correspond to a deformation without the internal strain:

$$c_{11}'=\sqrt{3}[\psi_{r^2}''(d^2)d/3+C_\theta/d^3]-P(d),$$

$$c_{12}'=\sqrt{3}[\psi_{r^2}''(d^2)d/3-C_\theta/2d^3]+P(d),$$

$$c_{44}'=\sqrt{3}[\psi_{r^2}''(d^2)d/3+C_\theta/6d^3]-P(d). \tag{B6}$$

The linear term in Eq. (B4) should be zero at equilibrium, $D=0$, which leads to Eq. (3.5). The internal strain must be eliminated from Eq. (B4) by minimization of the deformation energy. Deformation $u_1\neq 0$, or $u_2\neq 0$, or $u_3\neq 0$, or their combination does not lead to the appearance of internal strain. Thus, $c_{11}^*=c_{11}'$ and $c_{12}^*=c_{12}'$ and consequently we obtain Eq. (3.4a). Under deformation such as $u_4\neq 0$ the internal

strain appears, $\Delta\mathbf{u}=(-R/Q)(u_4,u_5,u_6)$. So, $c_{44}^{*}=c'_{44}-R^2/4Q$ and thence we obtain Eq. (3.4b).

3. Frequences of Γ, *X*, and *L* phonons

The phonon frequencies in the high-symmetry point may be obtained by the direct dynamic matrix calculation. For Γ-optic phonons:

$$\omega^2_{\mathrm{LTO}}(\Gamma)=8\frac{M_1+M_2}{M_1M_2}\left(\psi'_{r^2}(d^2)+\frac{2}{3}\psi''_{r^2}(d^2)d^2+\frac{4C_\theta}{3d^2}\right). \tag{B7}$$

The LA(X) and LO(X) modes are independent:

$$\omega^2_{\mathrm{LA,LO}}(X)=\frac{8}{M_{1,2}}\left(\psi'_{r^2}(d^2)+\frac{2}{3}\psi''_{r^2}(d^2)d^2+\frac{5C_\theta}{3d^2}\right). \tag{B8}$$

The other frequencies of the six X and L modes can be obtaned from quadratic equations and expressed in the following form:

$$\omega^2_{\mathrm{O,A}}=\frac{1}{2M_1M_2}[F(M_1+M_2)\pm\sqrt{4M_1M_2H^2+F^2(M_1-M_2)^2}], \tag{B9}$$

where the corresponding force coefficients for transverse (T) and longitudinal (L) modes are

$$F_{\mathrm{T}(X)}=8\psi'_{r^2}(d^2)+(16/3)\psi''_{r^2}(d^2)d^2+20C_\theta/3d^2,$$

$$H_{\mathrm{T}(X)}=(16/3)[\psi''_{r^2}(d^2)d^2-C_\theta/d^2], \tag{B10}$$

$$F_{\mathrm{L}(L)}=8\psi'_{r^2}(d^2)+(16/3)\psi''_{r^2}(d^2)d^2+32C_\theta/3d^2,$$

$$H_{\mathrm{L}(L)}=4\psi'_{r^2}(d^2)-(8/3)\psi''_{r^2}(d^2)d^2+32C_\theta/3d^2, \tag{B11}$$

$$F_{\mathrm{T}(L)}=8\psi'_{r^2}(d^2)+(16/3)\psi''_{r^2}(d^2)d^2+26C_\theta/3d^2,$$

$$H_{\mathrm{T}(L)}=4\psi'_{r^2}(d^2)+(16/3)\psi''_{r^2}(d^2)d^2+8C_\theta/3d^2. \tag{B12}$$

For IV group semiconductors Eq. (B9) is simplified, $\omega^2_{\mathrm{O,A}}=(1/M)(F\pm H)$. In particular, we obtain Eq. (3.6).

4. TA(Γ−*X*) branch under high pressure

The dynamic matrix calculation gives TO and TA branches for the [1,0,0] direction [wave vector $\mathbf{k}=(k,0,0)$] in the following form:

$$\omega^2_{\mathrm{TO,TA}}=(1/M)(F_1\pm\sqrt{F_2^2+F_3^2}), \tag{B13}$$

where

$$F_1=8\psi'_{r^2}(d^2)+\frac{16}{3}\psi''_{r^2}(d^2)d^2+\left[\frac{26}{3}+2\cos\left(\frac{ka}{2}\right)\right]\frac{C_\theta}{d^2},$$

$$F_2=\cos(ka/4)\left(8\psi'_{r^2}(d^2)+\frac{16}{3}\psi''_{r^2}(d^2)d^2+\frac{32C_\theta}{3d^2}\right),$$

$$F_3=\sin(ka/4)\left(\frac{16}{3}\psi''_{r^2}(d^2)d^2-\frac{16C_\theta}{3d^2}\right). \tag{B14}$$

The experimental room-pressure data for the TA(Γ−X) branch may be used to determine the $C_{\theta 0}(k)$ dependence. In this case $\psi'_{r^2}(d_0^2)=0$. Having evaluated the experimental data for Si,[56] we obtain the evolution of the TA(X) branch under pressure (Fig. 3). Note, that the approach applied here for the approximation of $C_{\theta 0}(\mathbf{k})$ gives different limits of $C_{\theta 0}$ in the Γ point for different directions of a reciprocal lattice.

[1] W.L. Jonson, Prog. Mater. Sci. **30**, 81 (1986).
[2] See, for example, the review article by E.G. Ponyatovsky and O.I. Barcalov, Mater. Sci. Rep. **8**, 147 (1992).
[3] O. Mishima, L.D. Calvert, and E. Whalley, Nature (London) **314**, 76 (1985).
[4] R.J. Hemley, A.P. Jephcoat, H.K. Mao, L.C. Ming, and M.H. Manghnani, Nature (London) **334**, 52 (1988).
[5] D.D. Klug, Y.P. Handa, J.S. Tse, and E. Whalley, J. Chem. Phys. **90**, 2390 (1989).
[6] V.V. Brazhkin, A.G. Lyapin, S.V. Popova, and R.N. Voloshin, JETP Lett. **56**, 152 (1992); Phys. Rev. B **51**, 7549 (1995).
[7] S.T. Weir, Y.K. Vohra, C.A. Vanberborgh, and A.L. Ruoff, Phys. Rev. B **39**, 1280 (1989).
[8] V.V. Brazhkin, S.V. Popova, and R.N. Voloshin, J. Non-Cryst. Solids **136**, 241 (1991).
[9] L.E. Mc Neil and M. Crimsditch, Phys. Rev. Lett. **68**, 83 (1992).
[10] K.J. Kingma, R.J. Hemley, H.K. Mao, and D.R. Veblen, Phys. Rev. Lett. **70**, 3927 (1993).
[11] M.B. Kruger and R. Jeanloz, Science **249**, 647 (1990).
[12] K.J. Kingma, C. Meade, R.J. Hemley, H.K. Mao, and D.R. Veblen, Science **259**, 666 (1993).
[13] M.B. Kruger, R. Jeanloz, M.P. Pasternak, R.D. Taylor, B.S. Snyder, A.M. Stacy, and S.R. Bohlen, Science **255**, 703 (1992).
[14] D. Wolf, R.P. Okamoto, S. Yip, J.F. Lutsko, and M. Kluge, J. Mater. Res. **5**, 286 (1990).
[15] J.S. Tse, J. Chem. Phys. **96**(7), 5482 (1992).
[16] J.S. Tse and D.D. Klug, Phys. Rev. Lett. **70**, 174, (1993).
[17] H. Sankaran, S.M. Sharma, S.K. Sikka, and R. Chidambaram, Prahana, J. Phys. **35**, 177 (1990).
[18] J. Wang, S. Yip, S.R. Phillpot, and D. Wolf, Phys. Rev. Lett. **71**, 4182 (1993).
[19] J. Wang, J. Li, S. Yip, S.R. Phillpot, and D. Wolf, Phys. Rev. B **52**, 12 627 (1995).
[20] N. Binggeli and J.R. Chelikowsky, Phys. Rev. Lett. **69**, 2220 (1992).

[21] N. Binggeli, N.R. Keskar, and J.R. Chelikowsky, Phys. Rev. B **49**, 3075 (1994).
[22] See references in J. Koike, Phys. Rev. B **47**, 7700 (1993).
[23] O.V. Stal'gorova, E.L. Gromnitskaya, and V.V. Brazhkin, JETP Lett. **62**, 356 (1995).
[24] R.G. Green, H. Luo, and A.L. Ruoff, Phys. Rev. Lett. **73**, 2476 (1994).
[25] M. Tang and S. Yip, Phys. Rev. Lett. **75**, 2738 (1995).
[26] M. Born and K. Huang, *Dynamical Theory of Crystal Lattices* (Clarendon, Oxford, 1954).
[27] W.A. Harrison, *Electronic Structure and the Properties of Solids* (Freeman, San Francisco, 1980).
[28] A.A. Maradudin, E.W. Montroll, and G.H. Weiss, *Theory of Lattice Dynamics in the Harmonic Approximation* (Academic, New York, 1963).
[29] If the initial atomic configuration **X** corresponds to a uniformly deformed crystal, the stress-strain coefficient tensor may be defined as $c^{*}_{\alpha\beta\gamma\lambda}=[\partial\sigma_{\alpha\beta}(\mathbf{X}')/\partial u_{\gamma\lambda}]_{\mathbf{X}}$, here $\sigma_{\alpha\beta}(\mathbf{X}')$ is the applied stress after deformation $\mathbf{X}\rightarrow\mathbf{X}'$. According to Refs. 18 and 30 $c^{*}_{\alpha\beta\gamma\lambda}=c_{\alpha\beta\gamma\lambda}+\frac{1}{2}[(\sigma_{\alpha\lambda}\delta_{\beta\gamma}+\sigma_{\beta\lambda}\delta_{\alpha\gamma}+\sigma_{\alpha\gamma}\delta_{\beta\lambda}+\sigma_{\beta\gamma}\delta_{\alpha\lambda})-2\sigma_{\alpha\beta}\delta_{\gamma\lambda}]_{\mathbf{X}}$, where $c_{\alpha\beta\gamma\lambda}=[V^{-1}\partial^{2}F(\mathbf{X}',T)/\partial u_{\alpha\beta}\partial u_{\gamma\lambda}]_{\mathbf{X}}$. Here $F(\mathbf{X}',T)$ is the free energy of a crystal.
[30] D.C. Wallace, *Thermodynamics of Crystals* (Wiley, New York, 1972).
[31] $1\equiv xx$, $2\equiv yy$, $3\equiv zz$, $4\equiv yz$, $5\equiv zx$, and $6\equiv xy$.
[32] V.V. Brazhkin and A.G. Lyapin, High Pressure Res. **15**, 9 (1996).
[33] *Rare Gas Solids*, edited by M.L. Klein and J.A. Venables (Academic, London, 1976), Vol. I.
[34] I.N. Frantsevich, F.F. Voronov, and S.A. Bokuta, *Elastic Constants and Elastic Moduli of Metals and Insulators* (Naukova dumka, Kiev, 1982).
[35] E.Yu. Tonkov, *High Pressure Phase Transformations* (Gordon and Breach, Philadelphia, 1992).
[36] S. Bhagavantam and J. Bhimasenachar, Proc. R. Soc. London Ser. A **187**, 381 (1946).
[37] R. Biswas and D.R. Haman, Phys. Rev. Lett. **55**, 2001 (1985); J. Tersoff, Phys. Rev. B **37**, 6991 (1988); B.C. Bolding and C. Andersen, *ibid.* **41**, 4005 (1990), and references therein.
[38] M.J.P. Musgrave and J.A. Pople, Proc. R. Soc. London Ser. A **268**, 474 (1962).
[39] R.M. Martin, Phys. Rev. B **1**, 4005 (1970).
[40] A.W. Solbrig, Jr., J. Phys. Chem. Solids **32**, 1761 (1971).
[41] *Numerical Data and Functional Relationships in Science and Technology*, edited by K.-H. Hellwege, Landolt-Börnstein, New Series, Group III, Vol. 17a (Springer-Verlag, Berlin, 1982); *ibid.*, edited by O. Modelung, Vol. 22a (Springer-Verlag, Berlin, 1986).
[42] W. Weber, Phys. Rev. Lett. **33**, 371 (1974).
[43] E.O. Kane, Phys. Rev. B **31**, 7865 (1985).
[44] S.T. Weir, Y.K. Vohra, C.A. Vanderborgh, and A.L. Ruoff, Phys. Rev. B **39**, 1280 (1989).
[45] K. Mizushima, S. Yip, and E. Kaxiras, Phys. Rev. B **50**, 14 952 (1994).
[46] B.A. Weinstein and R. Zallen, *Light Scattering in Solids*, edited by M. Cardona and G. Güntherodt (Springer-Verlag, Berlin, 1984); B.A. Weinstein and G.I. Piermarini, Phys. Rev. B **12**, 1172 (1972).
[47] M.T. Yin and M.L. Cohen, Phys. Rev. B **26**, 3259 (1982).
[48] A. Martin Pendas, V. Luana, J.M. Recio, E. Francisco, M.A. Blanco, and L.N. Kantorovich, Phys. Rev. B **49**, 3066 (1994).
[49] Y.K. Vohra, S.J. Duclos, and Arthur L. Ruoff, Phys. Rev. Lett. **54**, 570 (1985).
[50] M.I. Turchinskaya, T.M. Turusbekov, Yu.L. Alshevskii, and E.I. Estrin, Fiz. Tverd. Tela (Leningrad) **19**, 1505 (1977) [Sov. Phys. Solid State **19**, 879 (1977)].
[51] K. Kunc and R.M. Martin, Phys. Rev. B **24**, 2311 (1981).
[52] J.A. Majewski and P. Vogl, Phys. Rev. Lett. **57**, 1366 (1986).
[53] Y. Ida, Phys. Rev. B **187**, 951 (1969).
[54] N.M. Plakida and T. Siklos, Phys. Status Solidi **39**, 171 (1970).
[55] E.W. Kellermann, Philos. Trans. R. Soc. London Ser. A **238**, 513 (1940).
[56] G. Nilson and G. Nelin, Phys. Rev. B **6**, 3777 (1972).